

5 Modeling the Hot Flow Curve of Commercial Purity Coppers with Different Oxygen Levels

5.1 The Hot Flow Behavior

Although the purity of fire-refined copper can be of 99.9%, the relatively controlled residual composition may promote sensitive variations in the hot flow behavior and the final mechanical properties. The residual composition, particularly the oxygen content, has been shown to affect the hot flow curve [1, 2, 3]. At lower temperatures an increase in residual oxygen contents, at least up to 62ppm, increases the stress at a constant strain rate and a given strain value. However, at temperatures above 850°C, the residual composition of other elements affects to a lesser degree the flow stress, but instead the residual composition affects the dynamically recrystallized grain size. In general lower temperatures during dynamic recrystallization (DRX) favor a smaller dynamically recrystallized grain size, which improves room temperature mechanical properties. But at lower temperatures a higher stress response may be expected depending on the oxygen content. Also at lower temperatures oxygen in copper influences the stress necessary to produce the same dynamically recrystallized grain. As an example, during previous research [1, 3], compression at 800°C and 0.1s^{-1} of coppers A, B and, C with increasing oxygen levels produced an almost equivalent dynamically recrystallized grain sizes of 60 μm , 67 μm and 68 μm respectively, however the peak stresses were of 44.82MPa, 50.52MPa and, 57.68MPa respectively. The steady state stress also followed the same behavior. The relationship between the residual chemical composition and the hot flow curve may thus be of interest while controlling the final mechanical properties of a hot-formed copper. The dynamically recrystallized grain size is studied elsewhere [1,3]. As a first step to understand the latter control an evaluation of the effect of the residual elements on the high temperature stress-strain curve must be carried out. The aim of the present work is to characterize the parameters of known hot flow models, which can then be used to predict the compression hot flow curve of 99.9% pure copper with varying residual oxygen levels.

The prediction of a hot flow curve has been comprehensively separated into two parts: strain hardening and dynamic recovery and then by DRX. Commonly the strain at peak stress indicates the beginning of DRX on a stress-strain curve, however the onset of DRX occurs at a previous critical strain value. For purposes of modeling the stress-strain curve, knowledge of the critical strain value is not usually needed. As explained elsewhere [2] the peak and steady state stress models could use an apparent activation energy, Q_{app} , for prediction. However as shown on a latter chapter [3] increasing the value of the self-diffusion activation energy, Q_{sd} , as a mean to fit stress-strain data affected by another hardening mechanism is physically incorrect. The extra stress or back stress needed to overcome precipitates should be subtracted from the stress registered during the test. As has been shown from early on, at higher temperatures the self-diffusion of atoms governs the hot flow behavior [4]. And on a 99.9% pure copper the self-diffusion coefficient cannot increase to the levels suggested by the apparent activation energy. On this work a more physical approach is presented when modeling the stress-strain curve, also a validation of the model is done by comparison with the experimental hot flow curves.

5.2 Relevant Experimental Procedure

The experimental procedure here is the same as earlier [3] and is only briefly reviewed. The residual chemical composition of the three coppers selected is shown on Table 5.1 along with the initial grain size before the hot compression tests. The coppers selected had increasing oxygen content: copper A had 26 ppm of oxygen, copper B had 46 ppm of oxygen and, copper C had 62 ppm of oxygen. Among the most significant elements were Pb, Ni and Ag, which were present in most quantity in copper B, in intermediate quantity in copper C and in least quantity in copper A. Phosphorous was the most abundant element in these fire-refined coppers. Phosphorous helps prevent fragility after soldering or brazing in the deoxidized high phosphorous coppers (DHP). The material was supplied as surplus billet after a hot extrusion operation, which assures a dynamically recrystallized microstructure with presumably weak texture components that may influence the hardening behavior. The billets measured 231mm in diameter and 35mm in thickness. Cylindrical samples of 15 mm height and 10mm of diameter were machined from the latter billet. These samples were annealed in a controlled inert atmosphere at 950°C in order to promote the grain size listed on Table 5.1. The uniaxial hot compression tests were performed on a computer enhanced Instron 4507 electromechanical testing machine to attain constant true strain rate. Samples were also protected with a nitrogen flow during the compression tests inside the furnace chamber. The eight testing temperatures began at 950°C and decreased in 50°C intervals until 600°C. The strain rates tested at each temperature were $0.3s^{-1}$, $0.1s^{-1}$, $0.03s^{-1}$, $0.01s^{-1}$, $0.003s^{-1}$ and $0.001s^{-1}$. The total strain attained in each test was 0.8. At the end of every test, samples were quenched in cool water. The stress-strain data was analyzed and the characteristic coefficients and exponents in the constitutive equations of the established hot flow models were obtained.

Table 5.1. Chemical composition (ppm) of the three coppers studied and initial grain size d_0 (μm) at the beginning of the hot compression tests.

ppm	P	Sn	Pb	Ni	Ag	S	Fe	Zn	O	d_0
Cu A	297	86.2	63.5	31.7	30.8	22.0	17.2	15.6	26	637
Cu B	253	120	169	54.3	46.5	9.8	16.3	31.3	46	570
Cu C	153	63.3	133	40.0	37.7	10.1	15.5	13.4	62	530

5.3 Review of the Experimental Results

The true stress-true strain curves were typical of materials undergoing softening by dynamic recovery and, when conditions were appropriate softening by DRX. The flow curves at 600°C and 650°C were representative of softening exclusively due to dynamic recovery. The difference between each copper laid on the magnitude of the observable stresses. Under the same conditions of strain rate and temperature the peak stress attained by copper C was always the highest, followed by copper B and then copper A with the lowest peak stress value. The beginnings of dynamic recrystallization (noticeable softening after the peak stress) were first noticed on the hot flow curve of 650°C and $0.003s^{-1}$ for copper B. Both coppers B and C seemed to recrystallize dynamically at the next slowest strain rate of $0.001s^{-1}$. At 700°C an incomplete dynamic recrystallization (absence of a clear steady state stress) was noticed on most of the hot flow curves for the three coppers. Only at the slowest strain rates of 700°C was complete recrystallization apparent, but micrograph analysis showed that homogeneous

grain refinement was only reached for some of these strain rates. The tests conducted at 750°C showed single peak dynamic recrystallization independently of the strain rate considered. Second peak stresses after the maximum stress peak (cyclic dynamic recrystallization) were noticed at the slowest strain rates of the 800°C hot flow curves. Multiple peak dynamic recrystallization was a general observation on most of the tests carried out at 850°C, 900°C and, 950°C for the three coppers. Only at the highest strain rates (0.3s^{-1} , 0.1s^{-1}) of these latter temperatures, was dynamic recrystallization of the single peak type. The shape of the hot flow curves has been shown on the results chapter [3]. As a general feature and similar to the dynamic recovery case, the largest stresses observed under dynamic recrystallization conditions corresponded to copper C, followed by copper B and A.

5.4 Interdependency of Strain Rate, Temperature and Stress

The studies of high temperature creep lead to consider that the activation energy for creep, Q_{creep} , in metals was equivalent to the activation energy for self-diffusion, Q_{sd} , which ultimately controlled the deformation process [4]. Although creep tests measure the strain rate under constant stress conditions, the deformation mechanisms found under hot flow tests (constant strain rate) are the same, making inverse comparisons possible. One method to acknowledge the interdependency of steady state creep rate with temperature, T , and stress, σ , is the Zener-Hollomon parameter, which is written as

$$Z = \dot{\epsilon} \exp(Q/RT)$$

where R is the universal gas constant, $8.314\text{kJ/K}\cdot\text{mole}$. High temperatures and low strain rates produce a low Z value whereas low temperatures and high stresses produce a higher Z value. The activation energy, Q , is the value that normalizes the data, i.e. unifies the points. Stress values can be plotted against Z and one unified curve should be noticed. The self-diffusion activation energy for copper [5, 6, 7] is 197kJ/mole , however slightly different values may be found [8, 9], but bearing in mind the adequate correlation obtained on a latter chapter [3] while using 197kJ/mole then this value will continue to be used. On another work [10] the apparent activation energies for coppers A, B and C were calculated to be 213kJ/mole , 266kJ/mole and 278kJ/mole , respectively when using peak stress values, σ_p . However a more physical treatment calls for separation of the additional stresses or back stresses, σ_0 , attributed to other strengthening mechanisms different from the diffusion controlled glide and climb of dislocations. The equation used to determine the stress was

$$\left[\frac{\dot{\epsilon}}{D_{sd}(T)} \right]^{1/5} = A \sinh \left\{ \alpha \left[\frac{(\sigma - \sigma_0)}{E(T)} \right] \right\}, \quad (4.2)$$

where the diffusion coefficient, $D(T)$, normalizes the strain rate and the elastic modulus, $E(T)$, normalizes the registered stress. The diffusion is an Arrhenius equation that contains the activation energy for self-diffusion. Frost and Ashby [5] give a definition of both $D(T)$ and $E(T)$. The constants A and α determined using eq. 4.2 and for each copper are given in Table 5.2, where A_p and α_p correspond to the values obtained using

the peak stress, σ_p , and likewise A_{ss} and α_{ss} were obtained using the steady state stress, σ_{ss} . As expected among the 99.9% coppers, the values A and α are almost the same.

Table 5.2. Values of A and α from eq. 4.2 after subtracting the corresponding back stress described by equations 4.5 and 4.6 to predict the peak and steady state stresses. Also shown are the values of A and α using Q_{app} from ref. [2].

	A_p	α_p	A_{ss}	α_{ss}	Q [kJ/mole]
Copper A	438	1583	687	1209	$Q_{sd} = 197$
Copper B	437	1584	694	1199	$Q_{sd} = 197$
Copper C	437	1585	790	1079	$Q_{sd} = 197$
Copper A	562	1743	854	1385	$Q_{app} = 213$
Copper B	2146	1278	3277	1006	$Q_{app} = 266$
Copper C	1920	1409	45060	93	$Q_{app} = 278$

5.5 Modeling Strain Hardening and Dynamic Recovery

One early physically based model to describe the observed decrease of the strain-hardening rate value ($\Theta = \left[\frac{\partial \sigma}{\partial \varepsilon} \right]_{\dot{\varepsilon}, T}$) on a Θ - σ plot was proposed by Voce [11, 12, 13] and later given the physical justification by Kocks [13]. The model described the Θ - σ behavior as a linear equation with an intercept of Θ_0 at the ordinates, which was defined as the quotient of a theorized saturation stress, $\sigma_{Sat.}$, over a characteristic strain value, ε_C . The linear intercept at the abscissas was $\sigma_{Sat.}$, which is the stress value to where the stress-strain curve will tend (not reached in practice). The strain-hardening rate evolution as a function of stress and the integrated function of strain are

$$\Theta = \frac{\partial \sigma}{\partial \varepsilon} \Big|_{\dot{\varepsilon}, T} = \Theta_0 \left(1 - \frac{\sigma}{\sigma_{Sat.}} \right) \quad (5.1)$$

and

$$\sigma = \sigma_{Sat.} + (\sigma_0 - \sigma_{Sat.}) \exp\left(-\frac{\varepsilon - \varepsilon_0}{\varepsilon_C} \right) \quad (5.2)$$

where σ_0 is the measured yield stress, ε_0 is the strain history at the beginning of the test. Kocks also defined a relationship between the saturation stress and T and $\dot{\varepsilon}$. The initial strain-hardening rate, Θ_0 , has been found almost constant for most metals. A disadvantage of the latter Voce-Kocks model is that under certain conditions the Θ - σ curve does not follow a straight line, instead an asymptotic behavior is observed, as if a slow transition into stage IV was occurring.

The non-linearity of Θ - σ curve was noticed by several researchers, which suggested alternative hardening theories. Bergström [14, 15] theorized another evolution of dislocation density with the increase of strain and also was able to arrive to an expression that described stress as a function of strain. The Bergström model would have described an asymptotic behavior on the Θ - σ curve, however the theoretical basis assumed a direct variation of dislocation density, ρ , with strain, which is now understood to be dependent on the deformation mode [16] and the individual grain

orientation [17, 18]. Albeit considering a general ρ - ε relationship is a conceptual flaw, the Bergström model was capable of predicting the particular cases studied. Roberts [19] first raised the issue of the non-linearity of the Θ - σ curve and proposed another asymptotic equation, which did not mathematically resemble the Bergström equation. The Roberts model has not enjoyed much acceptance and few implementations can be found in literature.

Later Estrin and Mecking [20] presented an asymptotic type model as an alternative to the linear type Voce-Kocks model. Estrin and Mecking described the strain-hardening rate evolution and the integrated function of strain as

$$\Theta = \frac{\alpha^2 b \mu^2}{2 \sigma d} \left(\frac{\dot{\varepsilon}}{\dot{\varepsilon}_{hp}} \right)^{2/m} \left[1 - \left(\frac{\sigma}{\sigma_{Sat.}^*} \right)^2 \right] \quad (5.3)$$

and

$$\sigma = \left[\sigma_{Sat.}^{*2} + (\sigma_0^2 - \sigma_{Sat.}^{*2}) \exp\left(-\frac{\varepsilon - \varepsilon_0}{\varepsilon_C^*} \right) \right]^{1/2} \quad (5.4)$$

where a new saturation stress, $\sigma_{Sat.}^*$, was defined as well as a new characteristic strain value, ε_C^* . Estrin and Mecking alleged that in some materials the assumption that the mean free path of dislocations being proportional to $\rho^{1/2}$ needed to be abandoned, because the spacing between impenetrable obstacles (or sinks for dislocations), which determines the mean free path is a geometrically determined quantity. The distance a dislocation can travel on eq. 5.3 is d , which is geometrically determined either by grain size or by particle spacing. On eq. 5.3 b is the Burgers vector and μ is the shear modulus. The rest of the terms appearing on eq. 5.3 are constants to be determined. If the rest of the constants on eq. 5.3 are agglomerated into two constants, then the eq. 5.3 becomes

$$\Theta = A/\sigma - B\sigma, \quad (5.5)$$

which clearly shows the asymptotic behavior. More recently Laasraoui and Jonas [21], based on the models by Bergström and Estrin and Mecking, have presented a model to describe dynamic recovery during the first part of the hot flow curve before additional softening by DRX may occur.

Laasraoui and Jonas theorized that a metal hardens as the increasing density of dislocations finds its mobility reduced, because of dislocation-dislocation and dislocation-obstacle interactions. In the meantime a density of dislocations finds recovery, because the mean free path is long enough to allow dislocations to reach the grain border or the surface. Other dislocations dynamically recover when annihilation occurs between dislocations of opposite sign. Laasraoui and Jonas explained the dislocation evolution during strain in the same manner Estrin and Mecking [20] and Bergström [14, 15] by using an expression equivalent to

$$\partial \rho / \partial \varepsilon = U - \Omega \rho. \quad (5.6)$$

Bergström first employed the notation of U and Ω . According to Laasraoui and Jonas the term responsible for the hardening mechanism is U and the term responsible for the softening during strain is Ω . The quantity $\partial\rho/\partial\varepsilon$ represents the change in dislocation density as the strain changes. The physically based expression that directly relates the dislocation density, ρ , with stress, σ , is

$$\sigma = \alpha'\mu b(\rho)^{0.5} \quad (5.7)$$

where α' is a geometric constant (not to be confused with a constant α appearing on eq. 4.2), b is the burgers vector and again μ is the shear modulus. If eq. 5.7 is used to substitute ρ in eq. 5.6 then a constitutive equation of the form

$$\sigma = [\sigma_{Sat.}^{*2} + (\sigma_0^2 - \sigma_{Sat.}^{*2})\exp(-\Omega\varepsilon)]^{1/2} \quad (5.8)$$

can be obtained where

$$\sigma_0 = \alpha'\mu b(\rho_0)^{1/2} \quad (5.9)$$

and

$$\sigma_{Sat.}^* = \alpha'\mu b(U/\Omega)^{1/2}. \quad (5.10)$$

The stress σ_0 is the initial stress due to the initial dislocation density, which in annealed materials is almost zero. Equation 5.8 of the Laasraoui and Jonas model is equivalent to eq. 5.3 of the Estrin and Mecking model. And in a similar manner the determination of the new saturation stress, $\sigma_{Sat.}^*$, and the softening parameter Ω is performed through a non-linear fitting of eq. 5.5 on a Θ - σ plot where $A = 0.5\Omega\sigma_{Sat.}^{*2}$ and $B = 0.5\Omega$. A direct fitting of eq. 5.8 on a stress-strain plot is iteratively difficult. And sometimes, due to the noise generated when differentiating eq. 5.8 to obtain Θ , fitting eq. 5.5 is also difficult. The dependency of $\sigma_{Sat.}^*$ with strain rate and temperature was described by an expression of the form of eq. 4.2. A comparison of the Laasraoui and Jonas model (eq. 5.8) to the Estrin and Mecking model (eq. 5.4) shows that Ω equals $1/\varepsilon_c^*$. Unlike the Estrin and Mecking model the Laasraoui and Jonas model described the strain rate and temperature dependency of Ω by a power law expression of the form

$$\Omega = K_\Omega Z^{m_\Omega} \quad (5.11)$$

where K_Ω is a function of initial grain size, D_0 , so that $K_\Omega = A_\Omega D_0^{n_\Omega}$. The parameter Z is elevated to a constant exponent value, m_Ω . The flow stress on eq. 5.8, unlike on eq. 5.2, describes an asymptotic behavior on the Θ - σ plot and thereby capturing the experimental trends of some materials and conditions.

Prado and Cabrera [22, 23] to minimize the difficulties when determining Ω and $\sigma_{Sat.}^*$ proposed a model that reproduces well the stress-strain behavior when the difference between $\sigma_{Sat.}^*$ and σ_p is negligible. As a counterpart to equations 5.8 and

5.10, Prado and Cabrera proposed that stress during dynamic restoration could be expressed by a function of strain of the form

$$\sigma = [\sigma_p^2 + (\sigma_0^2 - \sigma_p^2)\exp(-\Omega_{CP}\varepsilon)]^{1/2} \quad (5.12)$$

and

$$\sigma_p = \alpha'\mu b(U_{CP}/\Omega_{CP})^{0.5} \quad (5.13)$$

where the softening parameter Ω_{CP} and the hardening parameter U_{CP} are also a function of Z in the form of

$$\Omega_{CP} = K_{\Omega_{CP}}Z^{m_{\Omega_{CP}}} \quad (5.14)$$

and

$$U_{CP}(\alpha'b)^2 = K_{U_{CP}}Z^{m_{U_{CP}}} \quad (5.15)$$

where $K_{\Omega_{CP}}$, $m_{\Omega_{CP}}$, $K_{U_{CP}}$ and $m_{U_{CP}}$ are constants to be determined. This work has determined the latter constants with the purpose of implementing the Cabrera and Prado model during restoration before DRX of the three coppers in study. Table 5.3 shows the coefficient and exponent appearing on eq. 5.14 for the commercial purity coppers studied. On fig. 5.1 the plot of Ω_{CP} versus the Zener-Hollomon parameter shows the normalizing effect of the self-diffusion activation energy.

The exponent $m_{\Omega_{CP}}$ decreased for precipitation-strengthened coppers however not in the order expected. The exponent $m_{\Omega_{CP}}$ is smaller in Cu B and Cu C than in Cu A, the precipitation free copper. However a lower value was obtained for Cu B instead of Cu C. The coefficient $K_{\Omega_{CP}}$ also increases for the two precipitation-hardened coppers, but again is higher for Cu B instead of Cu C. A similar non-conclusive relationship was

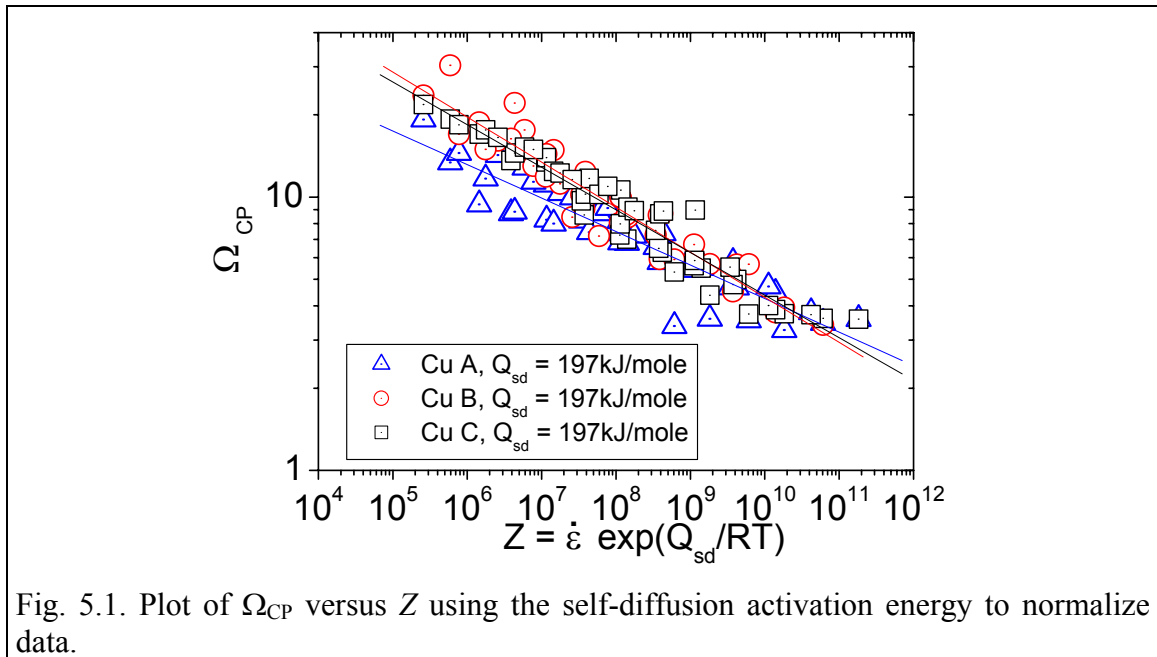


Fig. 5.1. Plot of Ω_{CP} versus Z using the self-diffusion activation energy to normalize data.

Table 5.3. Characteristic coefficients of the softening term Ω_{CP} for the coppers studied.

	$K_{\Omega_{CP}}$	$m_{\Omega_{CP}}$	Q [kJ/mole]
Copper A	78.66	-0.13	$Q_{sd} = 197$
Copper B	223.47	-0.17	$Q_{sd} = 197$
Copper C	158.87	-0.16	$Q_{sd} = 197$
Copper A	80.90	-0.12	$Q_{app} = 213$
Copper B	277.29	-0.13	$Q_{app} = 266$
Copper C	285.56	-0.13	$Q_{app} = 278$

Table 5.4 Characteristic coefficients of the hardening term $U_{CP}(\alpha'b)^2$ on eq. 5.15 for the coppers studied.

	K_{UCP}	m_{UCP}	Q [kJ/mole]
Copper A	1.95×10^{-7}	0.21	$Q_{sd} = 197$
Copper B	2.41×10^{-7}	0.24	$Q_{sd} = 197$
Copper C	2.24×10^{-7}	0.25	$Q_{sd} = 197$
Copper A	1.69×10^{-7}	0.20	$Q_{app} = 213$
Copper B	1.14×10^{-7}	0.19	$Q_{app} = 266$
Copper C	9.21×10^{-8}	0.20	$Q_{app} = 278$

Table 5.5 Characteristic coefficients of eq. 5.16 and eq. 5.11.

	K_W	n_W	K_{Ω}	m_{Ω}	Q [kJ/mole]
Copper A	88.60	-0.11	177.21	-0.11	$Q_{sd} = 197$
Copper B	225.89	-0.14	451.78	-0.14	$Q_{sd} = 197$
Copper C	207.90	-0.14	415.80	-0.14	$Q_{sd} = 197$
Copper A	98.25	-0.11	196.50	-0.11	$Q_{app} = 213$
Copper B	316.93	-0.11	633.86	-0.11	$Q_{app} = 266$
Copper C	347.38	-0.11	694.77	-0.11	$Q_{app} = 278$

found with the hardening parameter U_{CP} , here expressed as $U_{CP}(\alpha'b)^2$. Equation 5.15 shows the expression found between the Zener-Hollomon parameter and $U_{CP}(\alpha'b)^2$. Table 5.4 shows the coefficient and exponent values of the hardening parameter $U_{CP}(\alpha'b)^2$ for the commercial purity coppers studied. The value of $U_{CP}(\alpha'b)^2$ is of speculative importance, because eq. 5.12 of the model does not require an evaluation to determine σ . The coefficients and exponents for eq. 5.15 are close in value; only allow pointing out that the exponent m_{UCP} increases as the oxygen level increases. The coefficients and exponents that describe the softening and hardening parameters change when a copper is affected by precipitation hardening however an ordered correlation was not found.

Comparison of the reliability between models is not the objective of this work, however with a divulging character in mind the value of Ω according to Laasroui and Jonas (eq. 5.8) has been indirectly calculated. Estrin and Mecking [20] mathematically compared the Voce-Kocks model [13] with their model and explained that the term ε_C is equal to $2\varepsilon_C^*$. In the Laasraoui and Jonas model the term Ω is equal to $1/\varepsilon_C^*$. The present author for on-going research purposes has calculated ε_C for the three coppers, but instead has defined ε_C as

$$W = \frac{1}{\varepsilon_C} = K_W Z^{n_W} \quad (5.16)$$

where K_W and n_W are constants to be determined. The Ω parameter in the Laasraoui and Jonas model is then equal to $2W$. Table 5.5 shows the values of the characteristic constants that define W (eq. 5.16) and Ω (eq. 5.11). If desired for a future work the saturation stress, σ_{Sat} , which is not necessary for the Cabrera and Prado model, can be calculated using eq. 5.4, by inserting σ_p and ε_p , which can be defined using other relationships (eq. 4.2 and eq. 5.17). In a similar manner the new saturation stress, σ_{Sat}^* , can also be calculated using either eq. 5.4 or eq. 5.8. Regarding any of the restoration model equations 5.4, 5.8 or 5.12, the value of the peak stress is a function of strain; hence the point from where dynamic recrystallization is observed (on a stress-strain curve) is also strain dependent.

A relationship is needed to predict the strain at the peak stress, ε_p , where the onset of DRX on the stress-strain curve is first noticed. Like before a relationship with the Zener-Hollomon parameter has been found, such equation is as follows:

$$\varepsilon_p = K_\varepsilon Z^{m_\varepsilon} \quad (5.17)$$

The coefficient K_ε and the exponent m_ε were determined from a linear fit on a Log-Log plot of ε_p versus Z . Figure 5.2 shows the ε_p versus Z plot for the three coppers using the self-diffusion activation, Q_{sd} , which normalizes the strain data adequately well. Table 5.6 details the characteristic values of eq. 5.17. The coefficient K_ε decreases as the oxygen level increases. The coefficient m_ε of copper C is significantly higher than the other two coppers; this may be related to the higher stress values copper C reaches. Figure 5.2 also shows that the fitted lines intersect around $Z = 10^7 s^{-1}$ signaling a reverse effect of the oxygen on the peak strain. At higher Z values Cu C reaches higher peak strains, however that behavior reverses at lower Z values. Higher m_ε values produce higher ε_p values and thus the onset of dynamic recrystallization is delayed at high Z values in coppers bearing more residual oxygen.

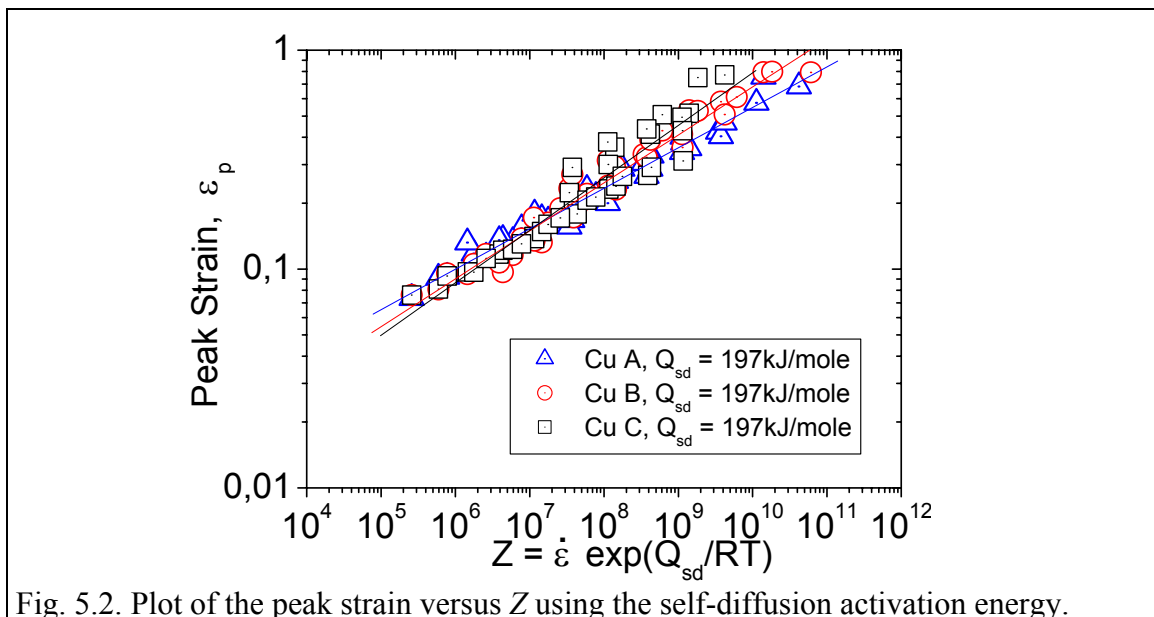


Fig. 5.2. Plot of the peak strain versus Z using the self-diffusion activation energy.

Table 5.6. Characteristic values of eq. 5.17 to predict the onset of DRX.

	K_ε	m_ε	Q [kJ/mole]
Copper A	6.571×10^{-3}	0.177	$Q_{app}=213$
Copper B	2.419×10^{-3}	0.175	$Q_{app}=266$
Copper C	1.338×10^{-3}	0.190	$Q_{app}=278$
Copper A	7.769×10^{-3}	0.185	$Q_{sd}=197$
Copper B	4.366×10^{-3}	0.219	$Q_{sd}=197$
Copper C	3.149×10^{-3}	0.240	$Q_{sd}=197$

5.6 Modeling Dynamic Recrystallization

On this part of work Dynamic Recrystallization (DRX) is modeled assuming that the softening on the flow curve is proportional to the recrystallized volume fraction, X . The difference between the peak stress, σ_p , and the steady state stress, σ_{ss} , are used to characterize the kinetics of DRX. A constitutive equation used earlier [10, 24, 22, 25] during DRX is

$$\sigma = \sigma_p - (\sigma_p - \sigma_{ss})X, \quad (5.18)$$

which is similar to others appearing in literature [26]. On eq. 5.18 stress is modeled to gradually decrease from the peak stress until reaching the steady state stress. The stress decreasing rate is determined by the recrystallizing volume fraction, X .

If Z and strain conditions allow (see eq. 5.17) then the deformed grain will begin to nucleate new low dislocation density grains, preferably on the triple grain junctions, borders, deformation bands and, hard particles. The new dynamically recrystallized grains represent a second softening mechanism (besides dynamic recovery) and normally consume the deformed grain from the border to the inside. The advancing recrystallized volume fraction, X , can be measured by an Avrami type equation first suggested for DRX by Lutton and Sellars [27] and can be written as

$$X = 1 - \exp(-K_A t^{n_A}) = 1 - \exp\left\{-0.693 \left[\frac{(\varepsilon - \varepsilon_p)}{\dot{\varepsilon} t_{50\%}} \right]^{n_A}\right\}. \quad (5.19)$$

Less error was made while measuring the time for DRX to consume 50% of the initial grain volume, $t_{50\%}$, and because $\exp(-0.693) \cong 0.5$ the relationship between the coefficient K_A and $t_{50\%}$ has remained as shown on eq. 5.19. If the softening observed on the stress-strain curve is proportional to the recrystallized volume fraction then

$$X = \frac{(\sigma_p - \sigma)}{(\sigma_p - \sigma_{ss})}. \quad (5.20)$$

On eq. 5.20 the stress σ is the registered stress during the hot compression test at constant strain rate. As a first step to characterize the kinetics of DRX the exponent n_A is calculated by measuring the slope on a $\ln\{\ln[1/(1-X)]\}$ versus $\ln[(\varepsilon - \varepsilon_p)(1/\dot{\varepsilon})]$ plot. Figures 5.3, 5.4 and 5.5 show the linear fitting sessions to calculate n_A for coppers A, B and, C respectively.

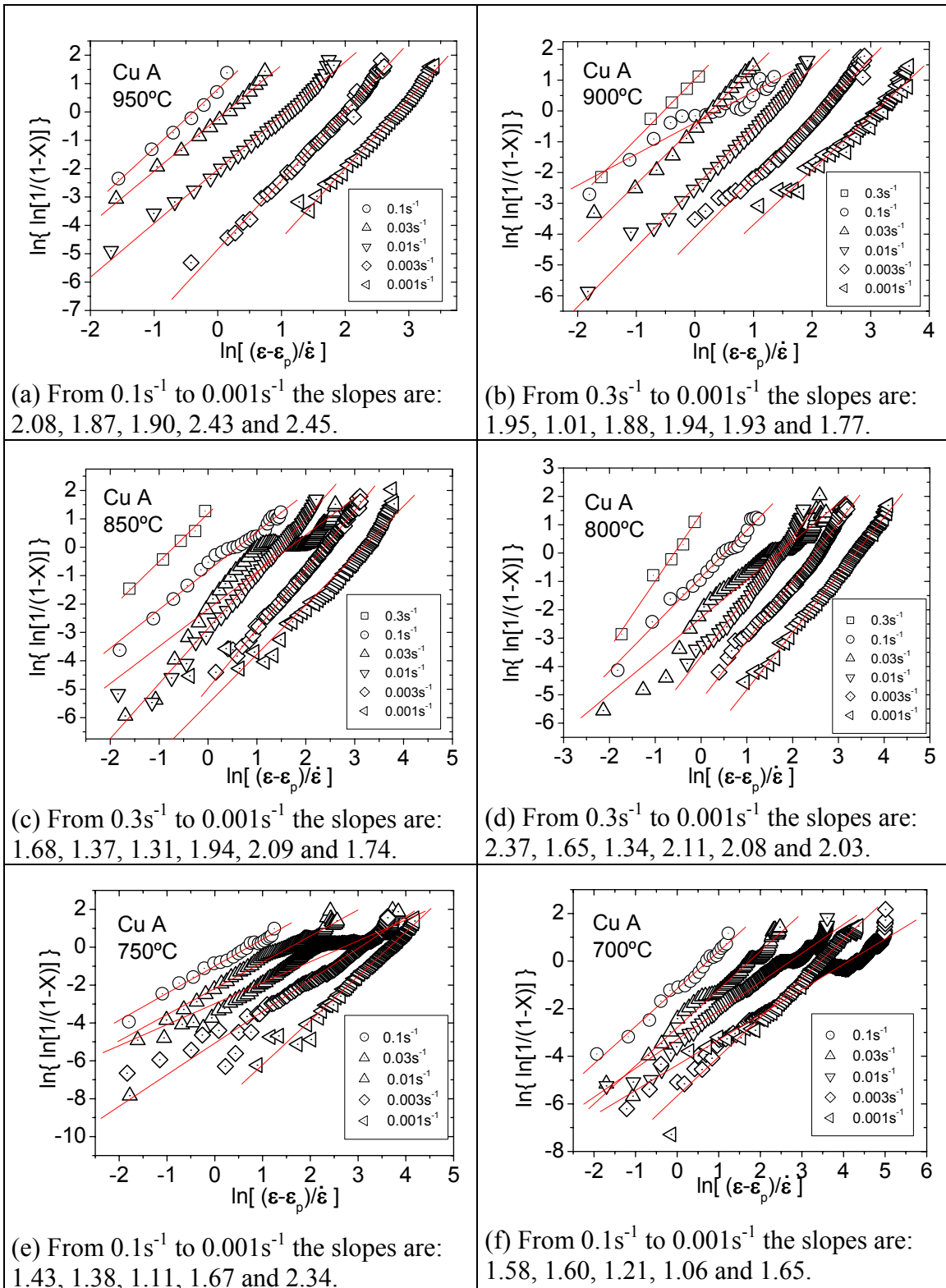


Fig. 5.3. Plots of $\ln\{\ln[1/(1-X)]\}$ versus $\ln[(\epsilon - \epsilon_p)/\dot{\epsilon}]$ for Cu A where the slope is equal to the Avrami exponent.

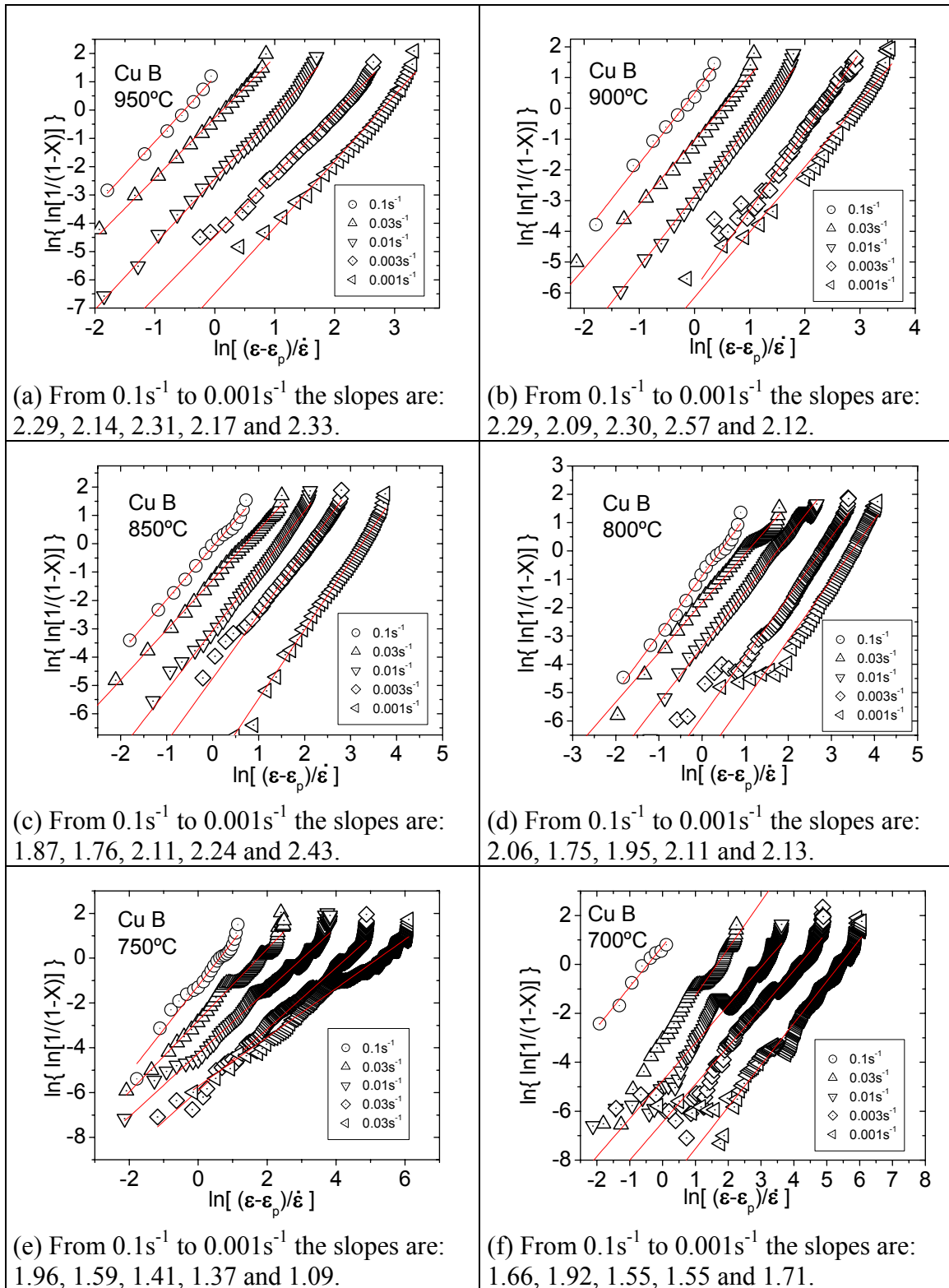


Fig. 5.4. Plots of $\ln\{\ln[1/(1-X)]\}$ versus $\ln[(\epsilon - \epsilon_p)/\dot{\epsilon}]$ for Cu B where the slope is equal to the Avrami exponent.

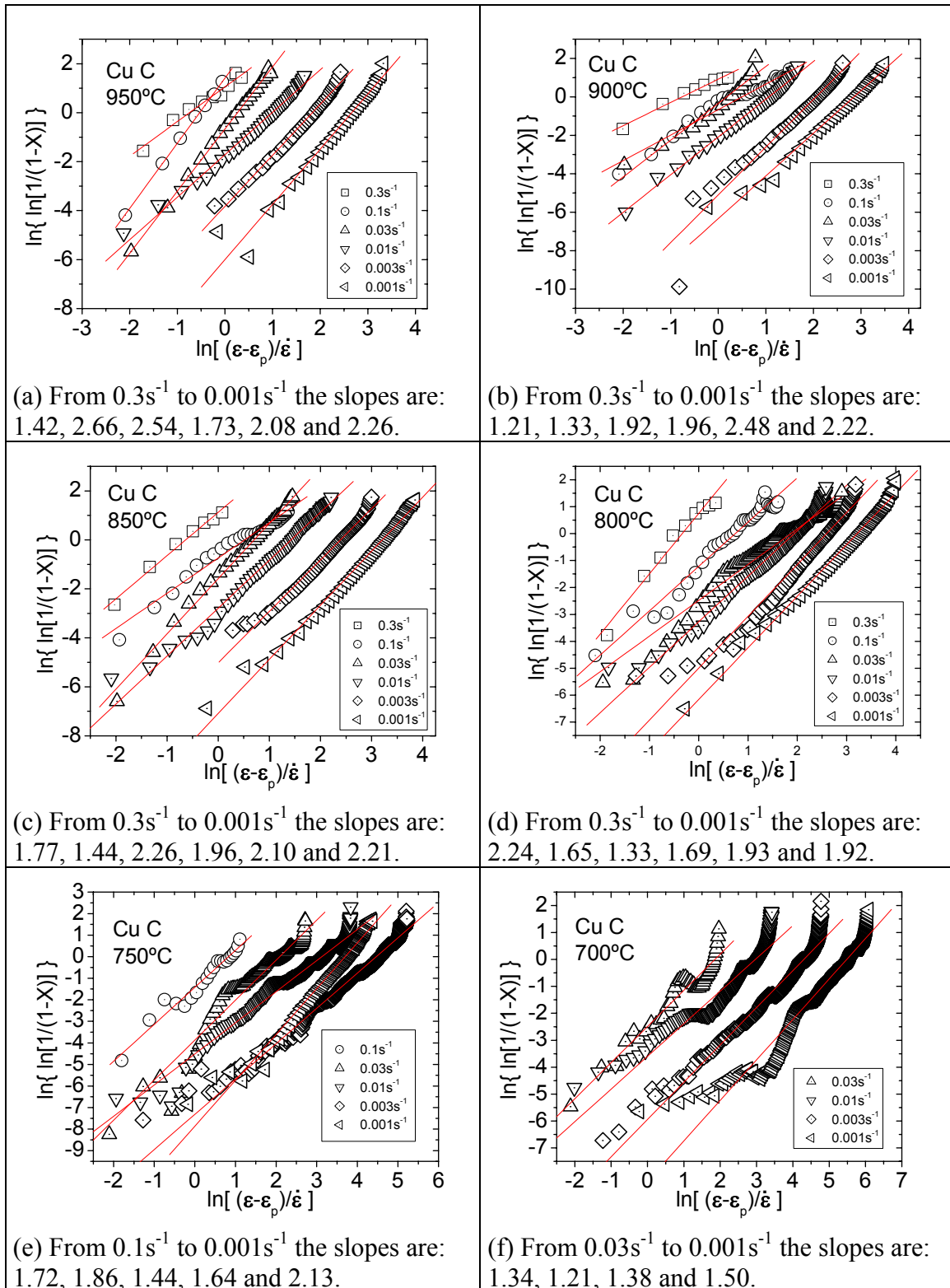


Fig. 5.5. Plots of $\ln\{\ln[1/(1-X)]\}$ versus $\ln[(\epsilon - \epsilon_p)/\dot{\epsilon}]$ for Cu C where the slope is equal to the Avrami exponent.

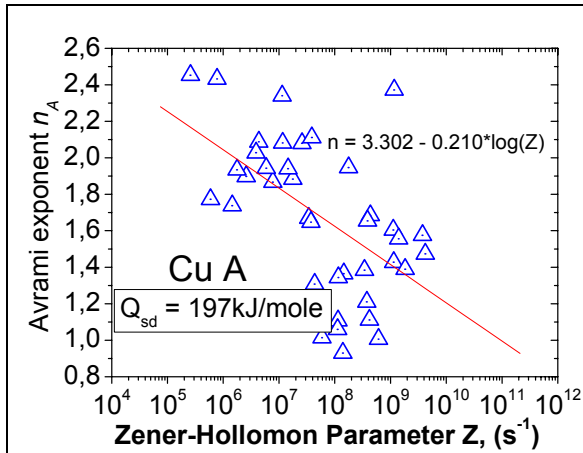


Fig. 5.6. The Avrami exponent versus Z using the self-diffusion activation energy for Cu A. The correlation is poor.

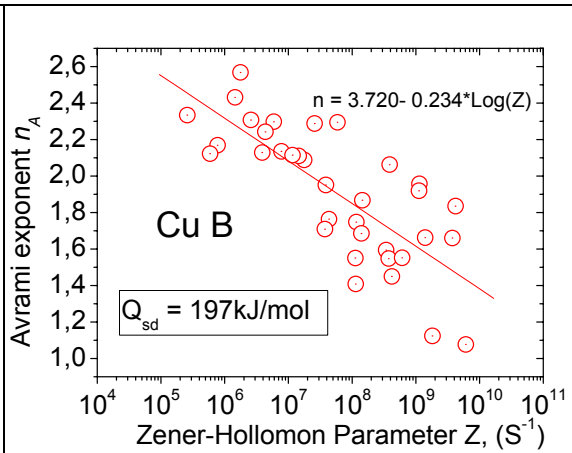


Fig. 5.7. The Avrami exponent versus Z using the self-diffusion activation energy. The correlation is not much different from fig. 5.6.

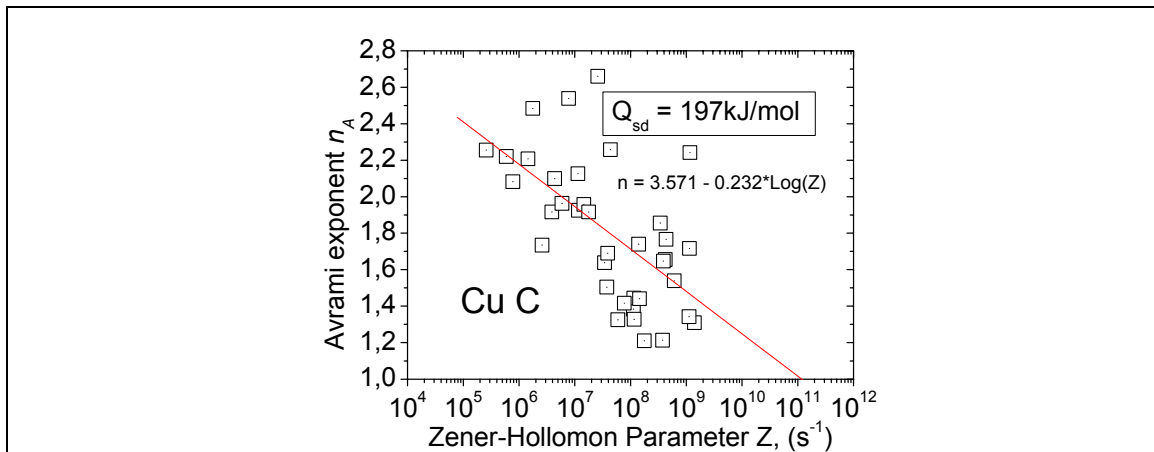


Fig. 5.8. The Avrami exponent versus Z using the self-diffusion energy for Cu C. As in fig. 5.6 and 5.7 the correlation is poor.

Then the n_A exponent is plotted against the Zener-Hollomon parameter as means of noticing an ordered behavior. The correlations between n_A and Z are poor either using Q_{app} or Q_{sd} , however the expression used to describe the change is

$$n_A = a_A + b_A \text{Log}Z, \quad (5.21)$$

where a_A and b_A are constants. Table 5.7 shows the values determined for the coefficients on eq. 5.21 calculated using Q_{sd} and Q_{app} . Figures 5.6, 5.7 and 5.8 show the n_A versus Z plot for Copper A, B and C respectively using Q_{sd} . The equation used earlier [10, 24, 22, 25] to characterize the time for recrystallization of 50% of the initial grain volume is

$$t_{50\%} = B_{50\%} \dot{\epsilon}^{m_{50\%}} \exp(Q_{50\%}/RT) \quad (5.22)$$

where $R = 8.314 \text{ kJ/K}\cdot\text{mole}$ is the universal gas constant, $B_{50\%}$ and $m_{50\%}$ are constant values to be determined as well as $Q_{50\%}$, another activation energy that controls the

Table 5.7. Characteristic values of eq. 5.21 to predict the Avrami exponent n_A .

	a_A	b_A	Q [kJ/mole]
Copper A	3.302	-0.210	$Q_{sd} = 197$
Copper B	3.720	-0.234	$Q_{sd} = 197$
Copper C	3.571	-0.232	$Q_{sd} = 197$
Copper A	3.416	-0.204	$Q_{app} = 213$
Copper B	4.089	-0.195	$Q_{app} = 266$
Copper C	3.971	-0.188	$Q_{app} = 278$

Table 5.8. Characteristic values of eq. 5.22 to predict $t_{50\%}$.

	$B_{50\%}$	$m_{50\%}$	$Q_{50\%}$
Copper A	3.82×10^{-3}	-0.61	40552
Copper B	5.00×10^{-5}	-0.93	68358
Copper C	1.44×10^{-3}	-0.72	50271

DRX process. Relationship 5.22 is independent of Q_{app} or Q_{sd} . Table 5.8 shows the values of the constants that characterize eq. 5.22. Coppers A and C present similar coefficients, but copper B separates substantially (see tables 5.7 and 5.8), this could be related to the fact that copper B produced on average finer recrystallized grain diameters. The hot flow behavior of the entire curve has been modeled. A comparison between the experimental hot flow curves and the predicted curves will help validate the reliability of the model applied on coppers with varying residual compositions. Strain hardening and dynamic recovery will be modeled using eq. 5.12 then the onset of DRX is indicated by eq. 5.17. When the peak strain occurs (eq. 5.17) the associated stress value, σ_{asc} , given by eq. 5.12 will begin to decrease at the rate given by eq. 5.19. And thus to couple constitutive eq. 5.12 with the constitutive equation during DRX, eq. 5.18 becomes

$$\sigma = \sigma_{asc} - (\sigma_{asc} - \sigma_{ss} + \sigma_{o_{ss}})X \quad (5.23)$$

where σ_{asc} is the stress value obtained by inserting ε_p (eq. 5.17) in eq. 5.12 and $\sigma_{o_{ss}}$ is the steady state back stress. The peak stress used on eq. 5.12 will also include the peak back stress (see appendixes A, B, C and D). An adequate prediction using only the self-diffusion activation energy was possible by separating the stress contributions of different hardening mechanisms. Figures 5.9, 5.10 and 5.11 show the comparisons of the predicted hot flow curves and the experimental curves for the three 99.9% pure coppers with varying residual oxygen amounts.

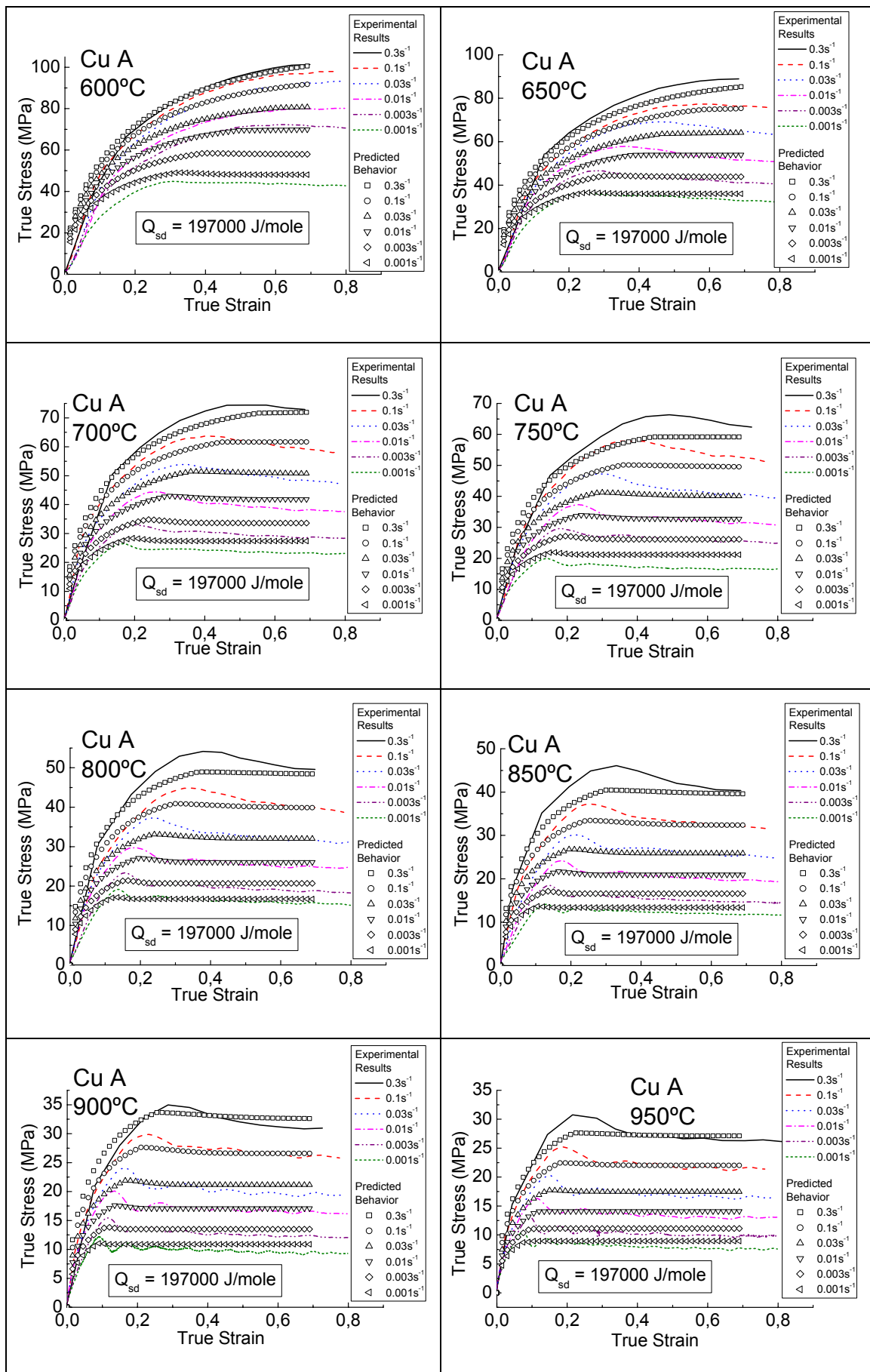


Fig 5.9. Comparison between the experimental and predicted hot flow curves for Cu A.

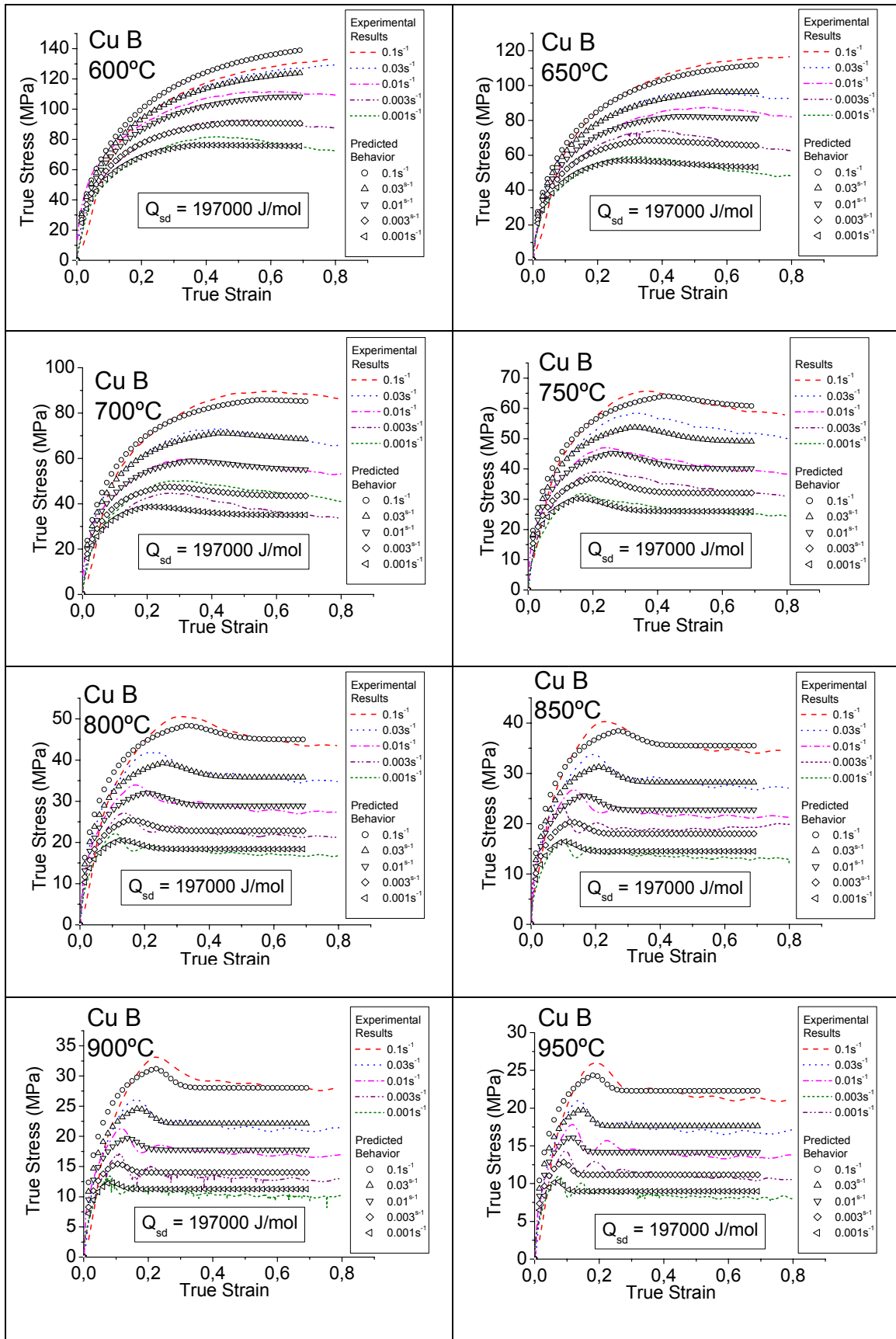


Fig. 5.10 Comparison between the experimental and predicted hot flow curves for Cu B.

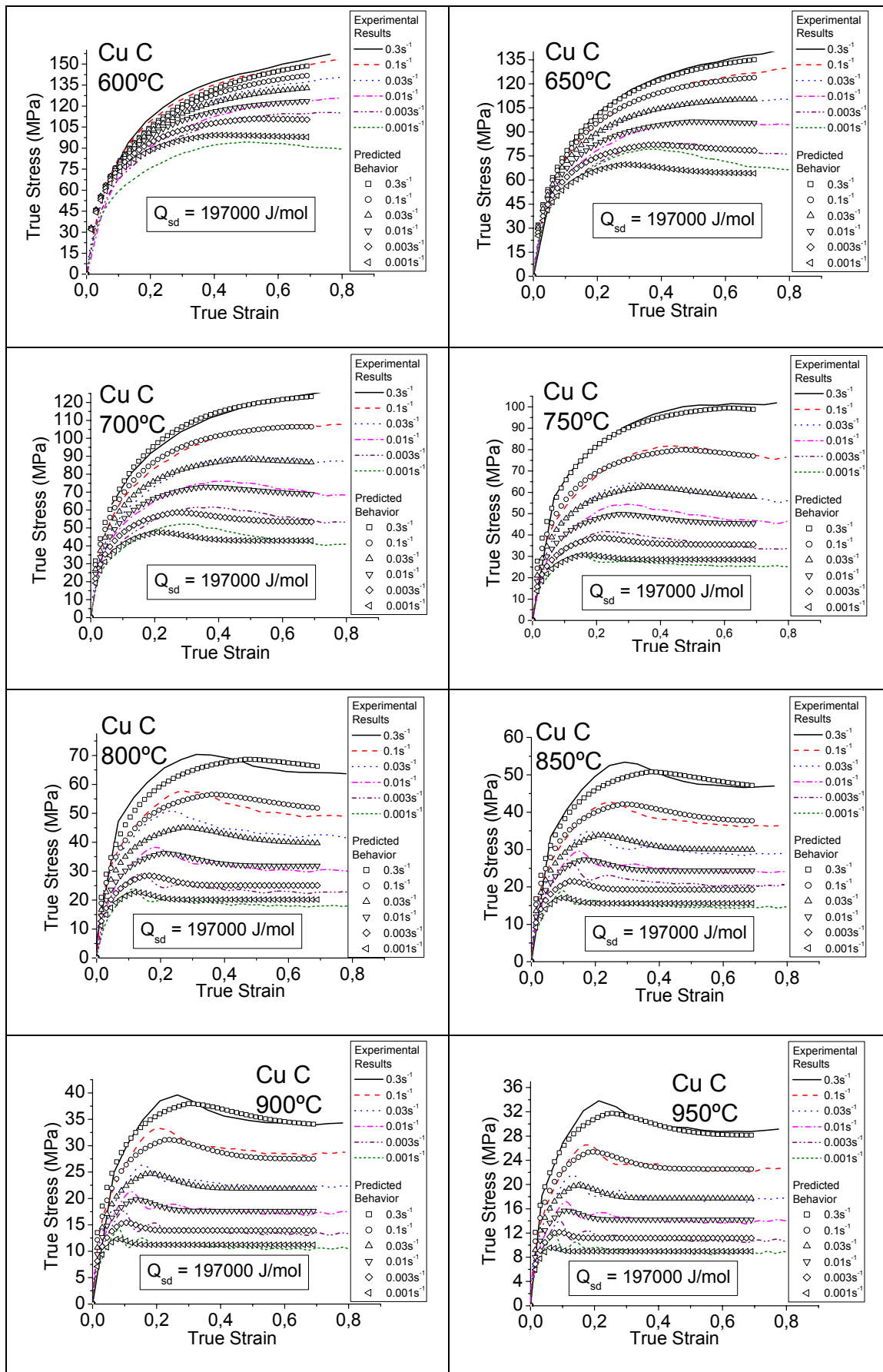


Fig. 5.11 Comparison between the experimental and predicted hot flow curves for Cu C.

5.7 Conclusions

A descriptive model of the hot flow curves of three commercial-purity coppers has been presented. The hot flow models selected are again [10, 24] validated on this work by a comparison with the experimental hot flow curves. The comparison demonstrates not only the reliability of the models, but also proves that using the self-diffusion activation energy is correct. At higher Z values The $\varepsilon_p - Z$ relationship showed that ε_p tends to be higher for the copper with higher oxygen content, however that effect reverses below $Z = 10^7 \text{s}^{-1}$. In the future a comparison between various hot flow models and using apparent activation energies may be done, as has been done elsewhere in literature [28].

5.8 Errata

The author assumes an unwilling error made while publicly reporting the simulation results using the self-diffusion activation energy. The error was on fig. 4 presented on references [10, 24] where instead of simulating strain hardening and dynamic recovery (eq. 5.12) with an expression for Ω_{CP} using eq. 5.14 ($K_{\Omega CP} = 78.66$, $m_{\Omega CP} = -0.127$) for copper A, an expression using non-linear fitted values for Cu B was used ($K_{\Omega CP} = 223.47$, $m_{\Omega CP} = -0.173$). The author uses a commercial worksheet to draw the simulated hot flow curve and once the erroneous fig.4 [10, 24] was completed, success appeared to have been reached and, no immediate verification was performed. The correct figure using the self-diffusion activation energy to correlate values with copper A and the models equations 5.12 and 5.14 is shown on fig. 5.9. An unfortunate and late conclusion is that fig. 5.9 is not as reliable as the erroneous figure.

5.9 References

- [1] García V.G., Cabrera J.M., Prado J.M., Dynamically Recrystallized Grain Size of Some Commercial Purity Coppers, Proceedings of the First Joint International Conference on Recrystallization and Grain Growth (Aachen), Eds. Gottstein G. And Molodov D.A., Springer-Verlag, Berlin, vol.1, (2001), pp.515-520.
- [2] García V.G., Cabrera J.M. and Prado J.M., Modeling the Hot Flow Stress of Commercial Purity Coppers with Different Oxygen Levels, Thermec'2003, Materials Science Forum, vols. 426-432 (2003), Trans Tech Publications, Switzerland, <http://www.scientific.net>, pp. 3921-3926.
- [3] García Fernández V.G., Ph. D. Thesis, Universitat Politècnica de Catalunya, Barcelona, Spain, (2004). <http://tdx.cesca.es>
- [4] Weertman Johannes, Dislocations Climb Theory of Steady-State Creep, Transactions of the ASM, Vol. 61, (1968) pp. 681-694.
- [5] Frost H.J., Ashby M.F., Deformation-Mechanism Maps, The Plasticity and Creep of Metals and Ceramics, Pergamon Press, Oxford, (1982), pp. 1-165.
- [6] Kuper A., Letaw Jr. H., Slifkin E., Sonder E., Tomizuka C.T., Self-Diffusion in

- Copper, Physical Review, vol. 96, no. 5, (1954), pp.1224-1225.
- [7] Kuper A., Letaw Jr. H., Slifkin E., Sonder E., Tomizuka C.T., Self-Diffusion in Copper (Errata), Physical Review, vol. 98, (1955), pp.1870.
- *[8] Neumann G., Tolle V., Philos. Mag., A 54, (1986), pg. 619.
- [9] Hoshino Kazutomo, Iijima Yoshiaki, Hirano Ken-Ichi, Solute Enhancement of Self-Diffusion of Copper in Copper-Tin, Copper-Indium, and Copper-Antimony Dilute Alloys, Acta Metallurgica, Vol. 30, (1982), pp. 265-271.
- [10] García V.G., Cabrera J.M., Riera L.M., Prado J.M., Hot Deformation of a Commercial Purity Copper, Proceedings of Euromat 2000: Advances in Mechanical Behaviour, Plasticity and Damage, vol. 2, Elsevier Science, Oxford, pp.1357-1362.
- *[11] Voce E., The Relationship Between Stress and Strain for Homogeneous Deformation, Journal of the Institute of Metals, vol. 74, (1948), pp. 537-562.
- *[12] Voce E., A Practical Strain-Hardening Function, Metallurgia, vol. 51, (1955), pp. 219-226.
- [13] Kocks U.F., Laws for Work-Hardening and Low-Temperature Creep, Journal of Engineering Materials and Technology Trans. AIME, Vol. 98, January (1976), pp. 76-85.
- [14] Bergström Y., A Dislocation Model for the Stress-Strain Behaviour of Polycrystalline α -Fe with Special Emphasis on the Variation of the Densities of Mobile and Immobile Dislocations, Materials Science and Engineering, ASM, vol. 5, (1969/70), pp. 193-200.
- [15] Bergström Y., Aronsson B., The Application of a Dislocation Model to the Strain and Temperature Dependence of the Strain Hardening Exponent n in the Ludwik-Hollomon Relation Between Stress and Strain in Mild Steels, Metallurgical Transactions, vol. 3, July (1972), pp. 1951-1957.
- [16] Ungár T, Tóth L.S., Illy J., Kovács I., Dislocation Structure and Work Hardening in Polycrystalline OFHC Copper Rods Deformed by Torsion and Tension, Acta metall. Vol. 34, No. 7, (1986), pp. 1257-1267.
- [17] Huang X., Grain Orientation Effect on Microstructure in Tensile Strained Copper, Scripta Materialia, Vol. 38, No. 11, (1998), pp. 1697-1703.
- [18] Huang X., Borrego A., Pantleon W., Polycrystal Deformation and Single Crystal Deformation: Dislocation Structure and Flow Stress in Copper, Materials Science and Engineering, A319-321, (2001) pp. 237-241.
- [19] Krauss George (editor), Deformation, Processing and Structure, 1982 ASM Materials Science Seminar, American Society for Metals, Metals Park, Ohio 44073, (1984), pp.i-524.

- [20] Estrin Y., Mecking H., A Unified Phenomenological Description of Work Hardening and Creep Based on One-Parameter Models, Acta Metall. Vol. 32, No. 1, (1984), pp. 57-70.
- [21] Laasraoui A., Jonas J.J., Prediction of Steel Flow Stresses at High Temperature and Strain Rates, Metallurgical Transactions A, Vol. 22A, July, (1991), pp. 1545-1558.
- [22] Cabrera J.M., Caracterización Mecánico-Metalúrgica de la Conformación en Caliente del Acero Microaleado de Medio Carbono 38MnSiVS5. Tesis Doctoral. Agosto (1995), Universidad Politécnica de Catalunya, Spain.
- [23] Cabrera J.M., Prado J.M., Simulación de la Fluencia en Caliente de un Acero Microaleado con un Contenido Medio de Carbono I parte. Aproximación Teórica, Rev. Metal Madrid, 33 (2), 1997, pp. 80-88.
- [24] García V.G., El Wahabi M., Cabrera J.M., Riera L.M., Prado J.M., Modelización de la Deformación en Caliente de un Cobre Puro Comercial, Rev. Metal. Madrid 37 (2001) ,pp.177-183
- [25] Cabrera J.M., Prado J.M., Simulación de la Fluencia en Caliente de un Acero Microaleado con un Contenido Medio de Carbono III parte.Ecuaciones Constitutivas, Rev. Metal Madrid, 33 (4), 1997, pp. 215-228.
- [26] Huang C., Hawbolt E.B., Chen X., Meadowcroft T.R., Matlock D.K., Flow Stress Modeling and Warm Rolling Simulation Behavior of Two Ti-Nb Interstitial-Free Steels in the Ferrite Region, Acta Materialia 49, (2001), pp. 1445-1452.
- [27] Luton M.J., Sellars C.M., Dynamic Recrystallization in Nickel and Nickel-Iron Alloys During High Temperature Deformation, Acta Metallurgica, vol. 17, (August 1969), pp. 1033-1043.
- [28] Tanner Albert B., McGinty Robert D., McDowell David L., Modeling Temperature and Strain Rate History Effects in OFHC Cu, International Journal of Plasticity, 15, (1999), pp. 575-603.

